



ORIGINAL PAPER

Linzi Fan · Yue Sun · Weiyin Fan · Yao Chen  · Jian Feng

# Determination of active members and zero-stress states for symmetric prestressed cable–strut structures

Received: 6 January 2020 / Revised: 2 April 2020 / Published online: 25 June 2020  
© Springer-Verlag GmbH Austria, part of Springer Nature 2020

**Abstract** A prestressed cable–strut structure is generally flexible and exhibits strong coupling between its stress state and configuration. The zero-stress state offers the basis for design and analysis of cable–strut structures and has significant influence on the prestress state and the load state. Here, a computational method is proposed for seeking zero-stress states of symmetric cable–strut structures. By evaluating distributed static indeterminacy and symmetry representations using group theory, the active member with proper importance index and high-order symmetry is chosen from different types of members. Moreover, natural lengths and the involved elongations of the members are established from the initial prestresses and geometric properties. Then, based on the Newton method and the Moore–Penrose inverse theory, internal forces of the members are actively reduced. The structural configuration and tangent stiffness matrix are iteratively updated during the whole process from the prestress state to the zero-stress state. The feasibility and accuracy of the proposed approach are verified by some numerical examples, whereas the results are compared with analytical solutions and FEM simulation. The results show that one zero-stress configuration is associated with a specific prestress state, and the process between zero-stress state and prestress state is reversible. This work has theoretical significance for the design of novel cable–strut structures and provides a reference for the construction process of prestressed cable–strut structures in practical applications.

## 1 Introduction

Cable–strut structures are mainly composed of tension cables and compression struts [1,2], and they are a class of prestressed pin-jointed assemblies that cannot be stable without introducing prestresses into the members [3,4]. Typical examples include tensegrity structures [5,6], and cable dome structures [3,7–9]. These structures are generally flexible and deployable [10,11] and exhibit strong coupling between the stress states and the structural configurations [12,13]. It is important to analyze the relationship between the configuration and stress states.

In the last two decades, morphology study has emerged as a prominent research area in the field of cable–strut structures [14–16]. Juan and Mirats Tur [17], Masic et al. [18], and Estrada et al. [19], respectively,

---

L. Fan  
School of Civil Engineering, Sanjiang University, Nanjing 210012, China

Y. Sun · W. Fan · J. Feng  
School of Civil Engineering, Southeast University, Nanjing 211189, China

Y. Chen (✉)  
Key Laboratory of Concrete and Prestressed Concrete Structures of Ministry of Education, and National Prestress Engineering Research Center, Southeast University, Nanjing 211189, China  
E-mail: chenyaoyao@seu.edu.cn

reviewed a few numerical form-finding methods for tensegrity structures. On the basis of the existing dynamic relaxation method [6], Miki et al. [20] generalized a geodesic dynamic relaxation method for cable–strut and membrane structures. Zhang and Ohsaki [15] introduced and improved the force density method for the form-finding of tensegrity structures. By repeatedly computing the force density matrices and the equilibrium matrices, Tran and Lee [4] proposed an iterative form-finding method for cable–strut structures. Later, Koohestani and Guest [21] described an analytical form-finding method for tensegrity, where the lengths of the members are taken as design variables. By effectively computing linear homogeneous systems in conjunction with a minimization problem, Feng [22] presented initial self-stress design of tensegrity grid structures. Based on group representation theory, Connelly and Back [23] explained mathematical principles behind tensegrities and adopted symmetry groups for presenting systematic classifications of 2D and 3D cable–strut structures. To further simplify the form-finding problem, Zhang and Ohsaki [24] and Chen et al. [25,26] developed group-theoretic approaches for prestressed cable–strut structures. Furthermore, with the development of metaheuristics [27], some optimization methods have been utilized to the form-finding problem of cable–strut structures [28,29]. For instance, the Monte Carlo form-finding method [30], the mixed integer nonlinear programming for tensegrity structures [31], and the form-finding techniques based on genetic algorithms [32] and ant colony optimization [33] have been successfully applied for robust form-finding of prestressed cable–strut structures.

Most of these form-finding methods focus on the prestressed equilibrium state (i.e., prestress state) of a structure, where the members are in tension or compression, and thus the structure states in self-stressed equilibrium. In fact, another type of equilibrium state should also be concerned for cable–strut structures, whereas the cables are just slack and contain zero stress [13,34]. This state is called as zero-stress state (unstressed state) [35], where the internal force of each member is zero. Notably, zero-stress state is a fundamental state among the stress states, and it is important for the design and structural analysis of a prestressed cable–strut structure [35]. In practice, a prestressed cable–strut structure is frequently formed by prestressing certain active members. Thereafter, the process of forming is like the prestressing process from the zero-stress state into the prestress state [36,37]. Therefore, zero-stress state is helpful for guiding the construction scheme of prestressed cable–strut structures. Moreover, it can significantly affect the involved prestress state and the load state, as the involved configurations are basically originated from the zero-stress state. However, the current research on cable–strut structures is mainly focused on form-finding [17,20,26], prestress design [38–40], load analysis [41,42], and active control [11,43]. There are very few studies on the zero-stress state of prestressed structures [35,36].

On the other hand, during structural analysis of a cable–strut structure using numerical methods or general FEM software, prestress state is frequently mistaken as the initial and unstressed state, and then prestressing is re-applied on the members [12,37]. As a result, the actual prestress state is not equivalent to the prestressed equilibrium state by form-finding. This phenomenon is called as configuration “drift” [35], which could be neglected for small-scale structures with low prestress level. Nevertheless, the zero-stress states should be exactly computed, to avoid such a phenomenon for the structures with high prestress level or high accuracy.

With regards to this, we will utilize the distributed static indeterminacy and symmetry analysis using group representation theory and propose a computational method to develop zero-stress states for symmetric cable–strut structures. A significance of this work is that active members are reasonably determined by simultaneously considering importance index and symmetry representations of the members in different symmetry orbits. Moreover, the Newton method and the Moore–Penrose inverse theory are introduced during the nonlinear computation process, to deal with matrix singularity induced by stiffness degradation. During the prestressing releasing process from the prestress state into the zero-stress state, the corresponding structural configuration and involved stiffness matrices need to be iteratively evaluated. The obtained zero-stress states will be verified by comparing the results with the analytical form-finding solutions and FEM simulation.

## 2 Zero-stress state of a prestressed cable–strut structure

### 2.1 Basic assumptions

Here, we adopt four basic assumptions for a general prestressed cable–strut structure:

- (i) The cable–strut structure states in a stable equilibrium because of being initially prestressed.
- (ii) All the members are connected via pin-joints and comprised of linear elastic materials.
- (iii) External loads and the self-weight of the structure are neglected during computing the zero-stress state.

(iv) The dynamic behavior of the whole system is not concerned.

### 2.2 Natural lengths of the members at zero stress

The above-mentioned assumptions point out a prestressed cable–strut structure should be stable under the prestressed equilibrium state, which can be effectively obtained from the existing form-finding process [26, 40, 44, 45]. After obtaining the prestressed equilibrium state, we can get the current length and the prestress (internal force) of each member in advance. Based on the second assumption, the axial stress of a member  $k$  is given by

$$\sigma_k = E_k \varepsilon_k \tag{1}$$

where  $E_k$  denotes the elastic modulus of the member  $k$ ,  $\sigma_k$  is the axial stress, and  $\varepsilon_k$  is the elastic strain. Further, the elastic strain  $\varepsilon_k$  can be written as

$$\varepsilon_k = \frac{l_k - l_{0k}}{l_{0k}} \tag{2}$$

where  $l_k$  is the stressed length at the prestressed equilibrium state, and  $l_{0k}$  is the natural length (length at zero stress) of the member  $k$ . As the stress  $\sigma_k$  is considered to be uniformly distributed in a member of the cable–strut structure, the axial force  $t_k$  of a strut (in compression) is expressed as

$$t_k = E_k A_k \varepsilon_k \tag{3}$$

where  $A_k$  is the cross-sectional area of the member  $k$ . Similarly, on condition that the member  $k$  acts as a tension cable, the axial force  $t_k$  is rewritten as

$$t_k = \begin{cases} E_k A_k \varepsilon_k & \text{if } l_k \geq l_{0k} \\ 0 & \text{otherwise} \end{cases} \tag{4}$$

to consider potential slackness of the cable when  $l_k < l_{0k}$ . By combining Eqs. (1)–(4), we calculate the natural length of the member  $k$ , given by

$$l_{0k} = \frac{E_k A_k}{E_k A_k + t_k} l_k \tag{5}$$

Then, the elongation  $\Delta l_k$  of this member is calculated by

$$\Delta l_k = l_k - l_{0k} = \frac{t_k l_k}{E_k A_k + t_k} \tag{6}$$

Equation (6) indicates that the natural length of every member at the zero-stress state keeps a constant value, when the prestressed equilibrium state is specified. Recall that the current length  $l_k$  and the prestress  $t_k$  of a general member  $k$  can be obtained by the existing form-finding process [26, 40, 44, 45], whereas the prestressed equilibrium state is developed in advance. To seek the zero-stress state of the cable–strut structure, the length and elongation of a member can be obtained from Eq. (6), whereas the structural configurations and the internal forces of the members need to be iteratively updated.

### 2.3 Nonlinear computation for the zero-stress state

Based on the equilibrium matrix theory [24, 46, 47], the equilibrium equation of all the free joints at the prestressed equilibrium state can be expressed in a compact matrix form,

$$\mathbf{H} \mathbf{t} = \mathbf{f}, \tag{7}$$

where  $\mathbf{H}$  is the equilibrium matrix,  $\mathbf{t}$  is the internal force (prestress) vector of the members, and  $\mathbf{f}$  the external load vector, which satisfies  $\mathbf{f} = \mathbf{0}$  at the prestressed equilibrium state.

To obtain the zero-stress state, a prestress cable–strut structure can be deliberately deformed from the equilibrium state by either moving the nodal positions (boundary constraints) or reducing the internal forces

of the members. In this study, the latter method is adopted, where the active members are chosen to actively reduce the internal forces. Because of the action of the active members and the induced force vector  $\mathbf{t}^*$ , the unbalanced forces at the pin-joints of the structure will be caused, given by

$$\mathbf{H}\mathbf{t}^* = \Delta\mathbf{f} \quad (8)$$

where  $\Delta\mathbf{f}$  denotes the unbalanced force vector. On the other hand, on the basis of the stiffness method [13,47,48], the unbalanced force vector  $\Delta\mathbf{f}$  can be rewritten as

$$\mathbf{K}_T\mathbf{d} = \Delta\mathbf{f}. \quad (9)$$

In Eq. (9),  $\mathbf{d}$  is the nodal displacement vector, and  $\mathbf{K}_T$  is the tangent stiffness matrix of the structure, which can be evaluated from

$$\mathbf{K}_T = \mathbf{H}\mathbf{G}\mathbf{H} + \mathbf{K}_G \quad (10)$$

where  $\mathbf{K}_G$  is the geometric stiffness matrix contributed by the internal forces of the members [37,49], and the  $b \times b$  diagonal matrix  $\mathbf{G}$  contains axial stiffness of the members, in which  $\mathbf{G}_{kk} = E_k A_k / l_{0k}$  and  $k \in [1, b]$ , and  $b$  is the total number of the members. Then, the nodal displacement vector can be predicted from Eq. (9),

$$\mathbf{d} = (\mathbf{K}_T)^+ \Delta\mathbf{f}, \quad (11)$$

where  $(\mathbf{K}_T)^+$  denotes the Moore–Penrose inverse of the tangent stiffness matrix  $\mathbf{K}_T$  [50], because the matrix tends to be ill-conditioned when the stress state of the cable–strut structure gets close to zero. Notably, during the stress release process transformed from the prestress state to the zero-stress state, the lengths of the cables are shortened, while the lengths of the struts are elongated [35]. Therefore, the nodal positions of the structure should be updated by

$$\mathbf{X} = \mathbf{X} + \mathbf{d} \quad (12)$$

where the vector  $\mathbf{X}$  describes the configuration of the evaluated structure. Because of strong coupling between the stress state and the configuration of the cable–strut structure, the obtained configuration is generally not associated with the expected zero-stress state. Thus, it is necessary to re-calculate the stress state of the structure.

Based on the current structural configuration given by Eq. (12), the internal forces  $\mathbf{t}^*$  of all the members (except for the active member) can be re-calculated, whereas

$$\mathbf{t}_{k \in [1, b]}^* = \begin{cases} 0 & \text{if member } k \text{ is a cable and } l_k^* \leq l_{0k} \\ E_k A_k (l_k^* - l_{0k}) / l_{0k} & \text{otherwise} \end{cases} \quad (13)$$

where  $l_k^*$  is the corresponding length of the member  $k$  obtained from the new configuration. By combining Eqs. (12)–(13) with Eqs. (8) and (10), the unbalanced force vector  $\Delta\mathbf{f}$  and the tangent stiffness matrix  $\mathbf{K}_T$  associated with the new configuration are evaluated. During the above-mentioned process, the internal force of the active member is deliberately reduced, and the stress state and configuration of the whole cable–strut system are gradually altered. As the motion path along the zero-stress state shows geometric nonlinearity, the Newton–Raphson technique is introduced to effectively approach the desired zero-stress state. Figure 1 shows a brief flowchart for computing the zero-stress state of a given cable–strut structure. Notably, the active member will be determined by the inherent symmetry representation and importance index of the members, which will be described in detail in Sect. 3. In addition, the structural configuration and the involved matrices of the input structure are iteratively updated, unless the internal force of each member approaches 0, i.e., the zero-stress state. Here, the convergence criteria for the zero-stress state are given by

$$\|\Delta\mathbf{f}\|_2 \leq \xi_0, \text{ and } \|\mathbf{t}\|_2 \leq \xi_0 \quad (14)$$

where  $\|\cdot\|_2$  denotes the 2-norm of a vector, and  $\xi_0$  denotes the tolerance to judge the zero-stress state ( $\xi_0 = 10^{-6}$  in this study). Note that the actual length of a member (except for the active member) at the zero-stress state should be equivalent to the natural/slack length of the member, which can be utilized to further verify the zero-stress configuration.

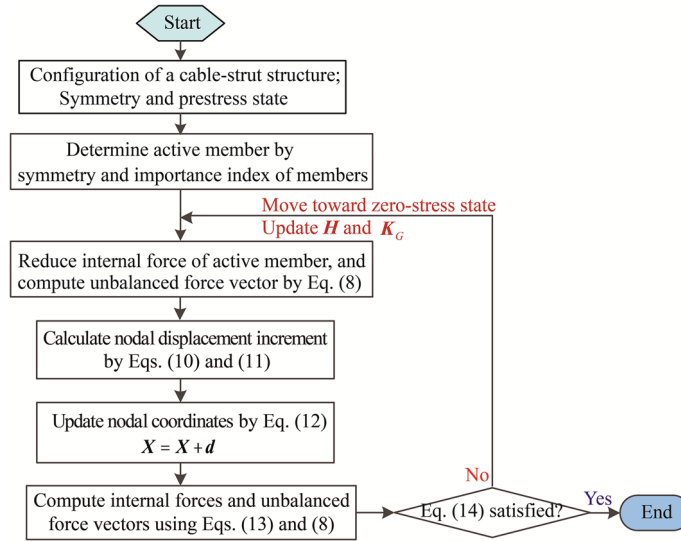


Fig. 1 Flowchart for computing the zero-stress state of a prestressed cable–strut structure

### 3 Determination of active members by their inherent symmetry and importance

#### 3.1 Symmetry representations for different types of members

For a structure with specific symmetry property, it keeps indistinguishable under a series of symmetry operations, where a member is moved along its symmetry orbit and located at the original position of certain members of the same type. Importantly, symmetry analysis using group representation theory [51,52] provides a systematic and robust approach for symmetry representations of different types of members. By recognizing unshifted members by the automated symmetry detection techniques [53,54], a vector  $\chi(b_k)$  for the  $k$ th type of unshifted members under symmetry operations is given by

$$\chi(b_k) = \{\chi_i \in [1, \tau]\}, \quad \forall k \in [1, t] \tag{15}$$

where  $t$  is the number of types of the members, the value  $\chi_i$  denotes the number of unshifted members under the  $i$ th symmetry operation, and the integer  $\tau \geq 2$  denotes the total number of independent symmetry operations for the structure. Based on the irreducible representations of a symmetry group and the vector  $\chi(b_k)$  shown in Eq. (15), we can get the symmetry representation  $\Gamma(b_k)$  for the  $k$ th type of members,

$$\Gamma(b_k) = \sum_{j=1}^{\mu} \beta_{b_k, j} \Gamma^{(j)}, \quad \forall k \in [1, t], \tag{16}$$

where the integer  $\beta_{b_k, j}$  is the weighting coefficient of the  $j$ th irreducible representation  $\Gamma^{(j)}$  for the  $k$ th type of members, and  $\mu$  is the total number of the irreducible representations for this symmetric structure. The smaller the number  $j$  shown in Eq. (16), the higher-order symmetry the representation  $\Gamma^{(j)}$  is associated with [55–57]. In fact, the representation  $\Gamma(b_k)$  offers an effective understanding on the symmetry behavior of the members of this type [55]. As far as an active member with a lower-order symmetry is concerned, the symmetric cable–strut structure necessarily breaks the original symmetry and retains partial symmetry operations [56,57]. In that case, symmetry variations induced by the active members can be effectively evaluated by their symmetry representation  $\Gamma(b_k)$ . Consequently,  $\Gamma(b_k)$  is utilized to predict the deformed configuration and internal forces of the structure and indicate symmetry descending of the initial perfect structure [58,59]. A member with a higher-order symmetry representation is likely to be chosen as the active member, which minimizes the impact on the configuration and stress states of the structure.

### 3.2 Importance index of a member

The importance index of a member plays a key role during the vulnerability or robustness analysis, which indicates a certain contribution of the involved member on the whole structure. As pointed out by recent studies [37,55,60], the stiffness-based importance index  $\alpha_{b_k}$  of a member of the  $k$ th type is complementary to the involved distributed static indeterminacy  $\gamma_{b_k}$ ,

$$\alpha_{b_k} = 1 - \gamma_{b_k}, \quad \forall k \in [1, t], \quad (17)$$

where the distributed static indeterminacy  $\gamma_{b_k}$  for the  $k$ th type members can be obtained from symmetry-adapted redundancy analysis [55],

$$\gamma_{b_k} = \frac{(\mathbf{V}_k^{(1)})^T \mathbf{G}^{-1} \mathbf{S} (\mathbf{S}^T \mathbf{G}^{-1} \mathbf{S})^{-1} \mathbf{S}^T \mathbf{V}_k^{(1)}}{n_{b_k}}, \quad \forall k \in [1, t] \quad (18)$$

where  $\mathbf{S}$  is a  $b \times s$  matrix including a total of  $s$  states of self-stress, and  $n_{b_k}$  is the total number of the  $k$ th type members. In Eq. (18), the  $b \times 1$  vector  $\mathbf{V}_k^{(1)}$ , which originates from the full symmetry subspace associated with the first irreducible representation  $\Gamma^{(1)}$ , is adopted for the  $k$ th type of members,

$$\mathbf{V}_{k,i}^{(1)} = \begin{cases} 1/\sqrt{n_{b_k}} & \text{if member } i \text{ belongs to the } k\text{th type} \\ 0 & \text{otherwise} \end{cases}, \quad \forall i \in [1, b], k \in [1, t]. \quad (19)$$

Note that the value  $\gamma_i = \gamma_{b_k}$  can demonstrate the impact of the adjacent members on a general member  $i \in [1, b]$  of the  $k$ th type. Notably, during form-finding analysis, the value of  $\gamma_{b_k}$  can be utilized to estimate the deformations and forces of the members caused by the initial elongation of the chosen member. For instance, a member  $i$  of the  $k$ th type is taken as the active member and subjected to an initial elongation  $e_{0i}$ , then the induced elongation  $e_i$  and the corresponding internal force  $t_i$  would be approximately evaluated by

$$e_i = -\gamma_i e_{0i}, \quad \text{and } t_i = -\mathbf{G}_{ii} \gamma_{b_k} e_{0i}, \quad \forall i \in [1, b] \quad (20)$$

where  $\gamma_i = \gamma_{b_k}$ , an extension  $e_{0i} > 0$  indicates axial compression, and a shortening  $e_{0i} < 0$  indicates tension. Equation (20) explains that a member can be less sensitive to the initial elongations, on condition that the value  $\gamma_{b_k}$  of this member is lower than that of another member. Therefore, a larger value of  $\gamma_{b_k}$  requires a stricter constraint on assembling the members of this type.

However, Eq. (17) reveals that the importance index  $\alpha_{b_k}$  of a member to load-bearing capacity gradually decreases with the rising  $\gamma_{b_k}$ . During developing or assembling a cable–strut structure, a member with a larger value of  $\alpha_{b_k}$  (or a smaller value of  $\gamma_{b_k}$ ) is more important than the other members, and thus they need to be more robust. Hence, when controlling or assembling a symmetric cable–strut structure, the members with either a larger  $\gamma_{b_k}$  or a smaller  $\gamma_{b_k}$  should not be chosen as the active members.

## 4 Numerical examples

To demonstrate high accuracy and efficiency of the proposed method for obtaining zero-stress states, several examples for symmetric cable–strut structures are studied and presented using MATLAB R2018a. In these examples, the elastic modulus of every member is denoted as  $E = 2.1 \times 10^5$  MPa.

### 4.1 A 2D cable–strut structure

A 2D cable–strut structure shown in Fig. 2a is taken as an example. This structure consists of four inclined cables (members 1–4), two horizontal cables (members 5–6), and two vertical struts (members 7–8). The lengths of the inclined cables, horizontal cables, and the struts are, respectively,  $2\sqrt{2}$  m, 3 m, and 4 m. All the tension cables have the same cross-sectional areas of  $A_c = 7.0686$  mm<sup>2</sup>, while the struts have the same cross-sectional areas of  $A_s = 113.0973$  mm<sup>2</sup>. Based on the integral feasible prestress mode using the form-finding method [26,40], the initial prestresses of the members at the prestressed equilibrium state are given by

$$t_{1-4} = 1.2\sqrt{2} \text{ kN}, \quad t_{5-6} = 1.2 \text{ kN}, \quad \text{and } t_{7-8} = -1.2 \text{ kN}. \quad (21)$$



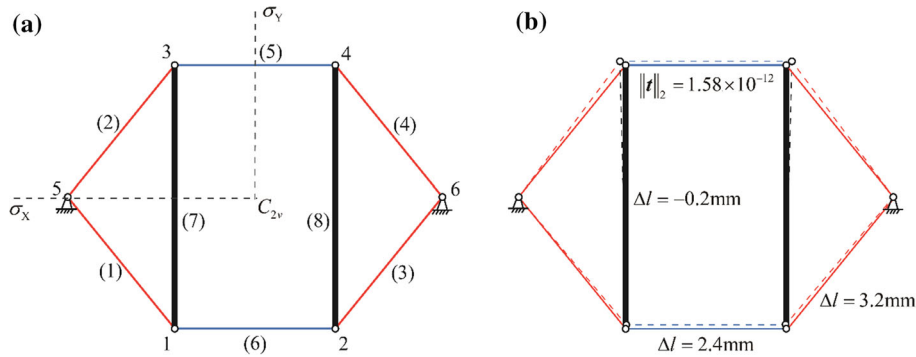


**Fig. 2** A 2D cable–strut structure with  $C_{2v}$  symmetry: **a** numbering of its nodes and members; **b** initial prestress state marked by the solid lines, and the obtained zero-stress state marked by the dotted lines

Figure 2a shows that the structure has  $C_{2v}$  symmetry, which keeps unchanged by  $\tau = 4$  symmetry operations (i.e., two rotations around the symmetry center, and two reflections  $\sigma_X$  and  $\sigma_Y$ ). After detecting the unshifted members with the automated symmetry detection method [53,54], we collect three reducible vectors for different types of members unshifted by the four symmetry operations

$$\chi(b_{1-4}) = \{4, 0, 0, 0\}, \quad \chi(b_{5-6}) = \{2, 0, 0, 2\}, \quad \chi(b_{7-8}) = \{2, 0, 2, 0\} \quad (22)$$

where  $\chi(b_{1-4})$ ,  $\chi(b_{5-6})$  and  $\chi(b_{7-8})$  denote the unshifted member vectors for the inclined cables, the horizontal cables, and the vertical cables, respectively. For instance, the first entry ‘2’ of  $\chi(b_{5-6})$  in Eq. (22) represents that the members 5–6 keep unshifted by the identity, while the last entry ‘2’ of  $\chi(b_{5-6})$  represents that the two members keep unshifted by the reflection  $\sigma_Y$ . The other entries can be explained in a similar way. On the basis of  $\mu = 4$  one-dimensional irreducible representations in the  $C_{2v}$  group, symmetry representations for different types of members can be obtained from Eq. (16),

$$\Gamma(b_{1-4}) = \Gamma^{(1)} + \Gamma^{(2)} + \Gamma^{(3)} + \Gamma^{(4)}, \quad \Gamma(b_{5-6}) = \Gamma^{(1)} + \Gamma^{(3)}, \quad \Gamma(b_{7-8}) = \Gamma^{(1)} + \Gamma^{(4)}, \quad (23)$$

where  $\Gamma^{(1)}$  denotes the first- and high-order representation with full symmetry, while  $\Gamma^{(4)}$  indicates the lowest-order symmetry. Equation (23) reveals that each member of the inclined cables shares a quarter of the full symmetry, while each of the horizontal cables and the struts shares a half of the full symmetry. Therefore, in comparison with the inclined cables, a member of the horizontal cables and the struts is more suitable as an active member. To further determine the active member from the importance index of the members, the distributed static indeterminacy of different types of members is evaluated by Eq. (18),

$$\gamma_{1-4} = 0.1944, \quad \gamma_{5-6} = 0.1027, \quad \gamma_{7-8} = 0.0085. \quad (24)$$

As given by Eq. (24), the members 5–6 with neither the maximum nor the minimum importance index can be considered as the active member. Thus, the horizontal cable 5 is adopted for the active member.

By the nonlinear computation procedure presented in Sect. 2, the whole process for obtaining zero-stress state terminates after five iteration steps. Thereafter, the 2-norm of the internal force vector of the members  $\|f\|_2 = 1.58 \times 10^{-12} < \xi_0$ . In other words, the members of the cable–strut structure approximately locate the zero-stress state. The obtained zero-stress configuration of the structure is illustrated in Fig. 2b. Evaluated lengths for the members have been listed in the first two columns in Table 1. It shows that the natural lengths

**Table 1** Lengths of members of the 2D cable–strut structure

Member no.	Stressed length $l_k$ (m)	Natural length $l_0$ (m)	Stressed length using FEM $l'_k$ (m)	Relative error between $l'_k$ and $l_k$ (%)
1–4	2.8284	2.8252	2.8286	0.007
6	3.0000	2.9976	3.0001	0.003
7–8	4.0000	4.0002	4.0000	0.000
5	3.0000	3.0211	2.9967	0.110

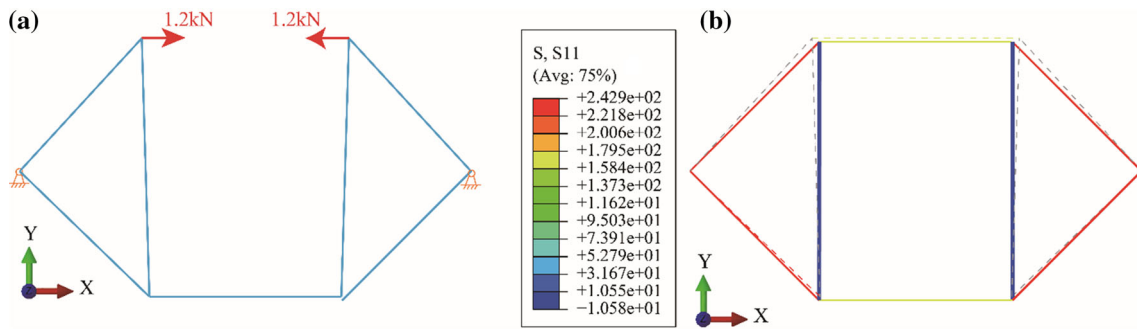


**Fig. 3** Finite element calculation of 2D cable–strut structure with  $C_{2v}$  symmetry: **a** FE model and its boundary conditions; **b** initial zero-stress configuration represented by dotted lines, and the prestressed configuration represented by solid lines

**Table 2** Internal forces of members of 2D cable–strut structure

Member no.	1, 3	2, 4	6	7–8	5
Prestress $t$ (kN)	1.6971	1.6971	1.2000	–1.2000	1.2000
Prestress $t'$ using FEM (kN)	1.7166	1.7150	1.2089	–1.1962	1.2000
Relative error (%)	1.149	1.055	0.742	0.317	0.000

of the members obtained from the final zero-stress configuration agree well with the analytical results given by Eq. (5).

On the other hand, if this cable–strut structure is prestressed from the zero-stress state by gradually tensioning the selected horizontal cable 5, the constructed configuration should be consistent with the given prestressed configuration shown in Fig. 2a. To verify the correctness of the proposed method, a finite element model for the zero-stress structural configuration is established, shown in Fig. 3a. As expected, the prestress is applied to the active member 5 of the zero-stress configuration, to allow the structure to be transformed into the prestressed equilibrium state.

The FEM results are shown in Fig. 3b, where the stresses of the members show that the struts are in compression at the prestress state, and the cables are in tension. It turns out that the inclined struts at the zero-stress state get vertical, after the structure reaches a stable equilibrium under the prestressing of the member 5. In addition, based on the FEM results, the stressed lengths and prestresses of the members at the prestress state are, respectively, listed in Tables 1 and 2. These results are compared with the analytic ones obtained by the form-finding method [53,54].

The results listed in Tables 1 and 2 show that stressed lengths and prestresses of all the members obtained from the form-finding method agree well with the FEM results. The maximum relative error of the lengths is 0.110%, while the maximum relative error of the prestresses is 1.149%. Thus, the proposed method has a satisfactory accuracy. Besides, Table 1 shows that the natural length of each passive cable is shorter than that of the cable at the prestress state, while the natural length of each strut is a bit longer than that of the strut at the prestress state. The distance between two nodes connecting the active cable is increased in the elastic state. The active cable is utilized to induce tension, and thus its natural length is longer than the stressed length at the prestress state.

Importantly, determination of active members significantly affects the zero-stress state of a cable–strut structure. Although the initial prestress state is identical, the obtained configuration of the structure with different active members can be different. To further explain this point, one of the horizontal cables, the active inclined cable, or the vertical struts are selected as the active member, and the corresponding zero-stress configuration is evaluated and shown in Fig. 4.

As expected, typical configurations shown in Fig. 4 are significantly different. Symmetry of the zero-stress configuration is determined by symmetry representation of the active member. The configurations shown in Fig. 4a, c keep mirror symmetry, while the configuration shown in Fig. 4b is asymmetric because of the lowest-order symmetry of the active inclined cable.



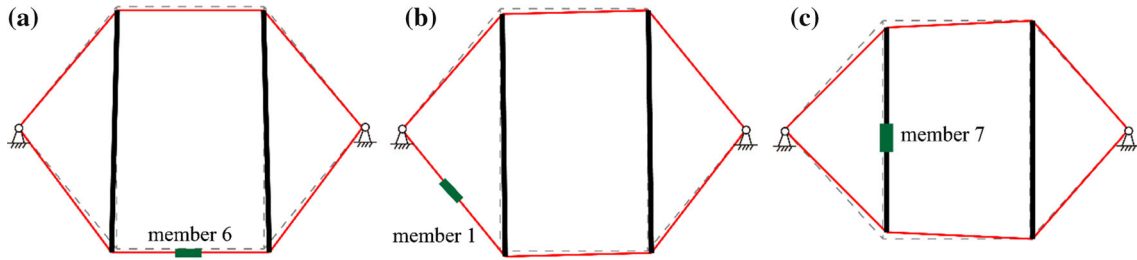


**Fig. 4** Different zero-stress configurations and symmetry induced by different active members: **a** an active horizontal cable; **b** an active inclined cable; **c** an active vertical strut

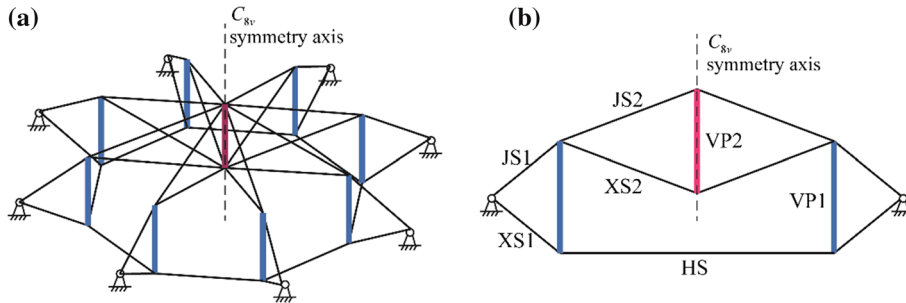


**Fig. 5** A  $C_{8v}$  symmetric cable dome structure with Geiger form: **a** 3D view; **b** different types of members in the section view

**Table 3** Distributed static indeterminacy and lengths of different types of members of a Geiger cable dome

Member	Cable					Strut	
	JS1	XS1	JS2	XS2	HS	VP1	VP2
$E_k A_k (\times 10^8 \text{ N})$	4.1233	4.1233	4.1233	4.1233	4.1233	10.2275	10.2275
$l_k \text{ (m)}$	9.2377	9.2377	16.5644	16.5644	12.2459	9.2380	8.5740
$t \text{ (kN)}$	879.5062	879.5062	394.2665	394.2665	995.1653	−439.7672	−816.3161

4.2 A Geiger cable dome with  $C_{8v}$  symmetry

A typical  $C_{8v}$  symmetric cable dome structure with the Geiger form [7] is shown in Fig. 5. It consists of 26 pin-joints, 40 cables and 9 struts, where eight outmost pin-joints are constrained along three directions. Such a structure exhibits  $C_{8v}$  symmetry [26,61], which has four one-dimensional irreducible representations,  $\Gamma^{(1)} - \Gamma^{(4)}$ , and three two-dimensional representations,  $\Gamma^{(5)} - \Gamma^{(7)}$  ( $\mu = 7$ ). Thus, the members can be classified by eightfold cyclic symmetry into  $t = 7$  types. As shown in Fig. 5b, JS1 and JS2 represent the upper ridge cables, XS1 and XS2 represent the lower diagonal cables, HS describes the hoop cables, and VP1 and VP2 represent the vertical struts.

This cable dome has a diameter of 48 m, and its equilibrium configuration subjected to initial prestresses has been reported by Xi et al. [39]. For clarity, Table 3 has listed the axial stiffness, stressed length, and prestress for different types of members of the  $C_{8v}$  symmetric cable dome.

To get symmetry representations of different types of the members, the number of unshifted members is evaluated for different kinds of symmetry operations. For the members JS1,

$$\frac{C_{8v} \text{ symmetry } E \quad 2C_8 \quad 2C_4 \quad 2C_8^3 \quad C_2 \quad 4\sigma_v \quad 4\sigma_d}{\chi(b_{JS1}) \quad 8 \quad 0 \quad 0 \quad 00 \quad 2 \quad 0} \quad (25)$$

where the first row indicates symmetry operations, and the corresponding value describes the number of unshifted cables JS1 under the operation. Based on Eq. (14), symmetry representation of the cables JS1 is

$$\Gamma(b_{JS1}) = \Gamma^{(1)} + \Gamma^{(3)} + \Gamma^{(5)} + \Gamma^{(6)} + \Gamma^{(7)}. \quad (26)$$

For the struts VP1 and the other cables, we have

$$\Gamma(b_{XS1}) = \Gamma(b_{JS2}) = \Gamma(b_{XS2}) = \Gamma(b_{HS}) = \Gamma(b_{VP1}) = \Gamma^{(1)} + \Gamma^{(3)} + \Gamma^{(5)} + \Gamma^{(6)} + \Gamma^{(7)} \quad (27)$$

**Table 4** Prestress and lengths for different types of members of Levy cable dome

Member	Cable					Strut	
	JS1	XS1	JS2	XS2	HS	VP1	VP2
$\gamma_{b_k}$	0.0274	0.0274	0.0099	0.0099	0.0465	0.0028	0.0088
$l_{0k}$ (m)	9.2180	9.2180	16.5485	16.5485	12.2164	9.2420	7.7561
$l'_{0k}$ (m)	9.2180	9.2180	16.5485	16.5485	12.2164	9.2420	8.5808

which are identical to the symmetry of the cables JS1. For the struts VP2,

$$\frac{C_{8v} \text{ symmetry } E \ 2C_8 \ 2C_4 \ 2C_8^3 \ C_2 \ 4\sigma_v \ 4\sigma_d}{\chi(b_{VP2}) \ 1 \ 1 \ 1 \ 1 \ 1 \ 1 \ 1}. \quad (28)$$

Thus, it can be reduced into

$$\Gamma(b_{VP2}) = \Gamma^{(1)} \quad (29)$$

which indicates that the strut VP2 holds full symmetry. Furthermore, the distributed static indeterminacy listed in Table 4 shows that the strut VP2 is neither the most important nor the most sensitive. Therefore, this member is considered as the active member.

To implement the nonlinear computation for zero-stress state, the prestressed equilibrium configuration shown in Fig. 5 is taken as the input configuration. The zero-stress configuration shown in Fig. 6a is obtained after 14 iteration steps, where the internal force vector satisfies  $\|t\|_2 = 3.37 \times 10^{-7} < \xi_0$ . Note that the structure maintains  $C_{8v}$  symmetry at the zero-stress state, with the active strut VP2 being released. The lengths of different types of members at the zero-stress state are reported in Table 4, where  $l_{0k}$  denotes the actual length of the member calculated from the zero-stress state, and  $l'_{0k}$  denotes the natural length analytically obtained by Eq. (5).

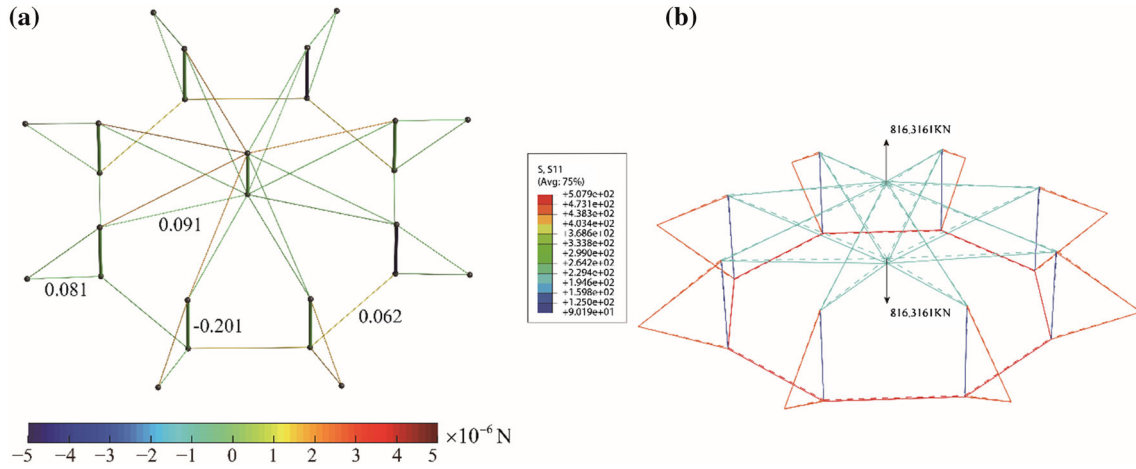
Both Fig. 6a and Table 4 describe that the obtained configuration locates exactly at the zero-stress state, whereas all the members are unstressed, and  $l_{0k} = l'_{0k}$  for the members except for the active strut VP2. Then, on the basis of the obtained zero-stress configuration, a FEM model using ABAQUS is established. Equivalent external loads are vertically applied at the ends of the strut VP2, to simulate the prestressing process and reach the equilibrium configuration. The FEM results are shown in Fig. 6b, where the solid lines indicate the equilibrium state and the dashed lines indicate the initial and zero-stress state.

It turns out that the FEM results are in good agreements with the analytical ones given in Table 3. The maximum relative error of the stressed lengths of the cables is 0.001% (JS1 or XS1), and the relative error of the lengths of the passive struts VP1 is 0.023%. In addition, the prestresses of different types of members calculated by FEM are shown in Fig. 7. The results are equivalent to those of the reported prestress state using the simplified force density method [39]. The maximum relative error of the prestresses of the cables is 0.203% (HS), and that of the prestresses of the struts is 0.077% (VP1). Thus, the zero-stress configuration is verified to be accurate, and the transformation between the zero-stress state and the prestress state is reversible.

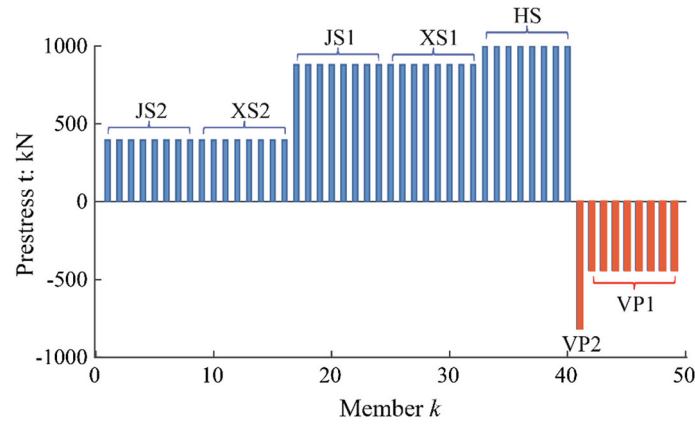
#### 4.3 A $C_{8v}$ symmetric cable dome structure with Levy form

Figure 8 shows another  $C_{8v}$  symmetric cable dome structure, which originates from the Levy form [8,40]. This structure consists of 26 pin-joints, 56 cables and 9 struts, where the eight outmost pin-joints are fully constrained. According to the inherent  $C_{8v}$  symmetry (eight reflections shown in Fig. 8b), the members are also classified into seven types. As shown in Fig. 8, members JS1 represent the upper ridge cables, XS1 represent the lower diagonal cables, and VP1 and VP2 represent the vertical struts. This structure is similar as the Geiger cable dome shown in Fig. 5, whereas the members JS1, XS1 and the lateral stiffness get improved.

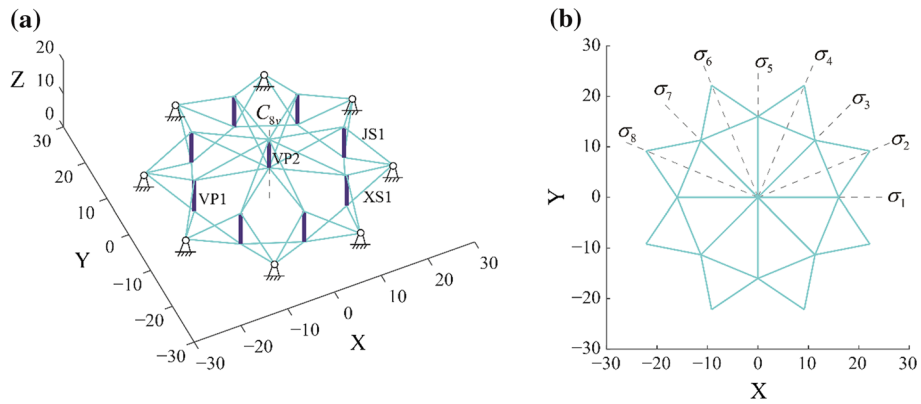
The prestress state of this symmetric Levy cable dome structure is obtained by the reported form-finding approach [26,40]. Initial prestresses and stressed lengths for different types of members are listed in Table 5. In the Table, distributed static indeterminacy  $\gamma_{b_k}$  of the members is also given. Because of the reasonable importance index and the full symmetry of the strut VP2, this member is considered as the active member, which is similar to that of the Geiger cable dome.



**Fig. 6** Stress states of the  $C_{8v}$  symmetric cable dome structure with Geiger form: **a** zero-stress configuration, and **b** prestress state and zero stress-state (dashed lines) obtained by FEM



**Fig. 7** Form-finding solutions of the  $C_{8v}$  symmetric Geiger cable dome

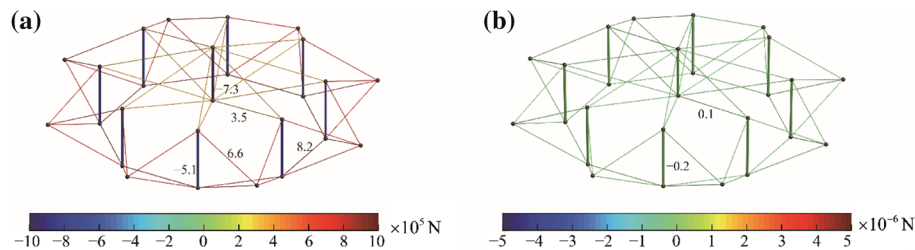
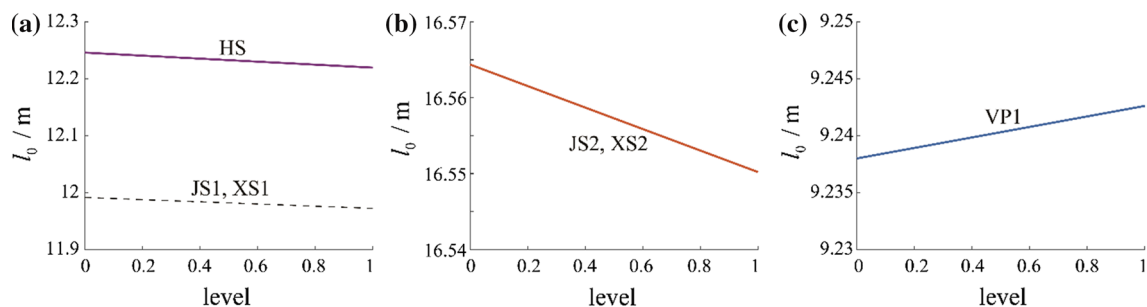


**Fig. 8** A  $C_{8v}$  symmetric cable dome structure with Levy form (unit: m): **a** 3D view, and **b** different symmetry operations in the plan view

Then, the zero-stress state is effectively obtained by the presented procedure. Figure 9a, b depicts the initial prestress state and the obtained zero-stress state, respectively. It can be easily observed that the absolute value of the internal force of every member is smaller than  $10^{-6}$  N. Moreover, the last row of Table 5 lists the natural lengths of different types of the members, which can be evaluated by the distance between the ends of the

**Table 5** Prestress and lengths for different types of members of Levy cable dome

Member	JS1	XS1	JS2	XS2	HS	VP1	Active strut VP2
$\gamma b_k$	0.0182	0.0182	0.0071	0.0071	0.0337	0.0034	0.0064
$t$ (kN)	662.3425	662.3425	352.9950	352.9950	890.9924	-510.2555	-730.8650
$l_k$ (m)	11.9915	11.9915	16.5644	16.5644	12.2459	9.2380	8.5740
$l_{0k}$ (m)	11.9723	11.9723	16.5502	16.5502	12.2195	9.2426	7.5455

**Fig. 9** Stress states of the Levy cable dome: **a** prestress state, and **b** zero-stress state**Fig. 10** Variations of natural lengths of different types of members affected by increasing prestress level: **a** cables HS, JS1 and XS2; **b** cables JS2 and XS2, and **c** strut VP1

members at the zero-stress state. We can verify that the natural lengths of the passive members accord with the analytical ones obtained by Eq. (5).

Recall that different zero-stress configurations of a structure can be obtained, on condition that the given prestress state is variable. To further investigate the influence of initial prestress on the evaluated zero-stress configuration, the input equilibrium configurations with different prestress levels are evaluated. Figure 10 shows the variations of natural lengths of different types of members affected by increasing prestress level.

As indicated by Eqs. (5) and (6), the higher the prestress level of the initial equilibrium state, the larger the deformation of a member becomes. Although the complete process between the prestress state and the zero-stress state is nonlinear, natural lengths of different types of cables/struts show linear decrease/increase affected by the rising prestress level.

## 5 Conclusions

Based on the Newton method and the Moore–Penrose inverse method, a computation method has been proposed for finding zero-stress states of symmetric prestressed cable–strut structures. To allow prestressing releasing from the stable equilibrium state, certain members are chosen to actively reduce the internal forces of the members. For a given symmetric cable–strut structure, the active member has been determined by considering its importance index and symmetry property.

Numerical examples show that the proposed approach has satisfactory accuracy, whereas the obtained results have been verified by the analytical form-finding solutions and FEM simulation. A series of zero-stress states of cable–strut structures can be effectively obtained by specifying symmetric and prestressed equilibrium states in advance. Each zero-stress configuration is associated with a specific prestressed equilibrium state, and the transformation between the prestress state and the zero-stress state is reversible. The presented work

is likely to help the design and analysis of various cable–strut structures and guides the practical prestressing process from the zero-stress state into the prestressed equilibrium state.

**Acknowledgements** This work has been supported by the National Natural Science Foundation of China (Grant Nos. 51978150 and 51850410513), the Southeast University “Zhongying Young Scholars” Project, and the Fundamental Research Funds for the Central Universities. Yao Chen would like to acknowledge financial support from the Alexander von Humboldt-Foundation for his visiting research at Max-Planck-Institut für Eisenforschung GmbH, Germany. The authors are grateful to the anonymous reviewers for their valuable comments.

## References

1. Wang, B.: Cable–strut systems: part II—cable–strut. *J. Constr. Steel Res.* **45**, 291–299 (1998)
2. Adam, B., Smith, I.: Tensegrity active control: multiobjective approach. *J. Comput. Civ. Eng.* **21**, 3–10 (2007)
3. Kawaguchi, M., Tatemichi, I., Chen, P.S.: Optimum shapes of a cable dome structure. *Eng. Struct.* **21**, 719–725 (1999)
4. Tran, H.C., Lee, J.: Advanced form-finding for cable–strut structures. *Int. J. Solids Struct.* **47**, 1785–1794 (2010)
5. Montuori, R., Skelton, R.E.: Globally stable tensegrity compressive structures for arbitrary complexity. *Compos. Struct.* **179**, 682–694 (2017)
6. Motro, R.: Tensegrity: Latest and Future Developments. In: Tensegrity, pp. 189–217. Butterworth-Heinemann, Oxford (2003)
7. Geiger, D.H., Stefaniuk, A., Chen, D.: The design and construction of two cable domes for the Korean Olympics. In: Proceedings of the IASS Symposium on Shells, Membranes and Space Frames, pp. 265–272. Elsevier Science Publishers BV, Osaka (1986)
8. Levy, M.P., Jing, T.F.: Floating saddle connections for the Georgia Dome, USA. *Struct. Eng. Int.* **4**, 148–150 (1994)
9. Quagliaroli, M., Malerba, P.G., Albertin, A., Pollini, N.: The role of prestress and its optimization in cable domes design. *Comput. Struct.* **161**, 17–30 (2015)
10. Fest, E., Shea, K., Domer, D., Smith, I.: Adjustable tensegrity structures. *J. Struct. Eng. ASCE* **129**, 515–526 (2003)
11. Veuve, N., Dalil Safaei, S., Smith, I.F.C.: Active control for mid-span connection of a deployable tensegrity footbridge. *Eng. Struct.* **112**, 245–255 (2016)
12. Zhang, P., Kawaguchi, K., Feng, J.: Prismatic tensegrity structures with additional cables: Integral symmetric states of self-stress and cable-controlled reconfiguration procedure. *Int. J. Solids Struct.* **51**, 4294–4306 (2014)
13. Chen, Y., Sun, Q., Feng, J.: Stiffness degradation of prestressed cable–strut structures observed from variations of lower frequencies. *Acta Mech.* **229**, 3319–3332 (2018)
14. Gasparini, D., Klinka, K.K., Arcaro, V.F.: A finite element for form-finding and static analysis of tensegrity structures. *J. Mech. Mater. Struct.* **6**, 1239–1253 (2011)
15. Zhang, J.Y., Ohsaki, M.: Adaptive force density method for form-finding problem of tensegrity structures. *Int. J. Solids Struct.* **43**, 5658–5673 (2006)
16. Lee, S., Lee, J.: Advanced automatic grouping for form-finding of tensegrity structures. *Struct. Multidiscipl. Optim.* **55**, 959–968 (2017)
17. Juan, S.H., Mirats Tur, J.: Tensegrity frameworks: static analysis review. *Mech. Mach. Theory* **43**, 859–881 (2008)
18. Masic, M., Skelton, R.E., Gill, P.E.: Algebraic tensegrity form-finding. *Int. J. Solids Struct.* **42**, 4833–4858 (2005)
19. Estrada, G.G., Bungartz, H.J., Mohrdieck, C.: Numerical form-finding of tensegrity structures. *Int. J. Solids Struct.* **43**, 6855–6868 (2006)
20. Miki, M., Adriaenssens, S., Igarashi, T., Kawaguchi, K.: The geodesic dynamic relaxation method for problems of equilibrium with equality constraint conditions. *Int. J. Numer. Methods Eng.* **99**, 682–710 (2014)
21. Koohestani, K., Guest, S.D.: A new approach to the analytical and numerical form-finding of tensegrity structures. *Int. J. Solids Struct.* **50**, 2995–3007 (2013)
22. Feng, X.: The optimal initial self-stress design for tensegrity grid structures. *Comput. Struct.* **193**, 21–30 (2017)
23. Connelly, R., Back, A.: Mathematics and Tensegrity: Group and representation theory make it possible to form a complete catalogue of “strut-cable” constructions with prescribed symmetries. *Am. Sci.* **86**, 142–151 (1998)
24. Zhang, J.Y., Ohsaki, M.: Self-equilibrium and stability of regular truncated tetrahedral tensegrity structures. *J. Mech. Phys. Solids* **60**, 1757–1770 (2012)
25. Chen, Y., Feng, J., Ma, R., Zhang, Y.: Efficient symmetry method for calculating integral prestress modes of statically indeterminate cable–strut structures. *J. Struct. Eng.* **141**, 04014240 (2015)
26. Chen, Y., Sun, Q., Feng, J.: Group-theoretical form-finding of cable–strut structures based on irreducible representations for rigid-body translations. *Int. J. Mech. Sci.* **144**, 205–215 (2018)
27. Kaveh, A., Bakhshpoori, T.: *Metaheuristics: Outlines, MATLAB Codes and Examples*. Springer, Switzerland (2019)
28. Rieffel, J., Valero-Cuevas, F., Lipson, H.: Automated discovery and optimization of large irregular tensegrity structures. *Comput. Struct.* **87**, 368–379 (2009)
29. Lee, S., Woo, B.H., Lee, J.: Self-stress design of tensegrity grid structures using genetic algorithm. *Int. J. Mech. Sci.* **79**, 38–46 (2014)
30. Li, Y., Feng, X.Q., Cao, Y.P., Gao, H.: A Monte Carlo form-finding method for large scale regular and irregular tensegrity structures. *Int. J. Solids Struct.* **47**, 1888–1898 (2010)
31. Xu, X., Wang, Y., Luo, Y.: Finding member connectivities and nodal positions of tensegrity structures based on force density method and mixed integer nonlinear programming. *Eng. Struct.* **166**, 240–250 (2018)
32. Koohestani, K.: Form-finding of tensegrity structures via genetic algorithm. *Int. J. Solids Struct.* **49**, 739–747 (2012)
33. Chen, Y., Feng, J., Wu, Y.: Novel form-finding of tensegrity structures using ant colony systems. *J. Mech. Robot.* **4**, 1283–1289 (2012)

34. Shekastehband, B., Abedi, K., Dianat, N., Chenaghlo, M.R.: Experimental and numerical studies on the collapse behavior of tensegrity systems considering cable rupture and strut collapse with snap-through. *Int. J. Nonlinear Mech.* **47**, 751–768 (2012)
35. Zhao, J., Chen, W., Fu, G., Li, R.: Computation method of zero-stress state of pneumatic stressed membrane structure. *Sci. China Technol. Sci.* **55**, 717–724 (2012)
36. Chen, L., Dong, S.: Optimal prestress design and construction technique of cable–strut tension structures with multi-overall selfstress modes. *Adv. Struct. Eng.* **16**, 1633–1644 (2013)
37. Chen, Y., Yan, J., Feng, J.: Stiffness contributions of tension structures evaluated from the levels of components and symmetry subspaces. *Mech. Res. Commun.* **100**, 103401 (2019)
38. Tran, H.C., Park, H.S., Lee, J.: A unique feasible mode of prestress design for cable domes. *Finite Elem. Anal. Des.* **59**, 44–54 (2012)
39. Xi, Y., Xi, Z., Qin, W.H.: Form-finding of cable domes by simplified force density method. *Proceedings of the Institution of Civil Engineers - Structures and Buildings* **164**, 181–195 (2011)
40. Chen, Y., Yan, J., Sareh, P., Feng, J.: Feasible prestress modes for cable–strut structures with multiple self-stress states using particle swarm optimization. *J. Comput. Civ. Eng.* **04020003** (2020)
41. Amendola, A., Carpentieri, G., de Oliveira, M., Skelton, R.E., Fraternali, F.: Experimental investigation of the softening–stiffening response of tensegrity prisms under compressive loading. *Compos. Struct.* **117**, 234–243 (2014)
42. Koohestani, K., Kaveh, A.: Efficient buckling and free vibration analysis of cyclically repeated space truss structures. *Finite Elem. Anal. Des.* **46**, 943–948 (2010)
43. Bel Hadj Ali, N., Rhode-Barbarigos, L., Smith, I.F.C.: Analysis of clustered tensegrity structures using a modified dynamic relaxation algorithm. *Int. J. Solids Struct.* **48**, 637–647 (2011)
44. Koohestani, K.: On the analytical form-finding of tensegrities. *Compos. Struct.* **166**, 114–119 (2017)
45. Zhang, J.Y., Ohsaki, M.: Force identification of prestressed pin-jointed structures. *Comput. Struct.* **89**, 2361–2368 (2011)
46. Pellegrino, S., Kwan, A., Vanheerden, T.F.: Reduction of equilibrium, compatibility and flexibility matrices, in the force method. *Int. J. Numer. Methods Eng.* **35**, 1219–1236 (1992)
47. Kovacs, F., Tarnai, T.: Two-dimensional analysis of bar-and-joint assemblies on a sphere: equilibrium, compatibility and stiffness. *Int. J. Solids Struct.* **46**, 1317–1325 (2009)
48. Zhang, P., Feng, J.: Initial prestress design and optimization of tensegrity systems based on symmetry and stiffness. *Int. J. Solids Struct.* **106**, 68–90 (2017)
49. Chen, Y., Feng, J.: Generalized eigenvalue analysis of symmetric prestressed structures using group theory. *J. Comput. Civ. Eng.* **26**, 488–497 (2012)
50. Chen, Y., Feng, J.: Efficient method for Moore–Penrose inverse problems involving symmetric structures based on group theory. *J. Comput. Civ. Eng.* **28**, 182–190 (2014)
51. Fowler, P.W., Guest, S.D.: A symmetry extension of Maxwell’s rule for rigidity of frames. *Int. J. Solids Struct.* **37**, 1793–1804 (2000)
52. Chen, Y., Feng, J., Liu, Y.: A group-theoretic approach to the mobility and kinematic of symmetric over-constrained structures. *Mech. Mach. Theory* **105**, 91–107 (2016)
53. Chen, Y., Sareh, P., Feng, J., Sun, Q.: A computational method for automated detection of engineering structures with cyclic symmetries. *Comput. Struct.* **191**, 153–164 (2017)
54. Zingoni, A.: Symmetry recognition in group-theoretic computational schemes for complex structural systems. *Comput. Struct.* **94–95**, 34–44 (2012)
55. Chen, Y., Feng, J., Lv, H., Sun, Q.: Symmetry representations and elastic redundancy for members of tensegrity structures. *Compos. Struct.* **203**, 672–680 (2018)
56. Chen, Y., Sareh, P., Feng, J.: Effective insights into the geometric stability of symmetric skeletal structures under symmetric variations. *Int. J. Solids Struct.* **69–70**, 277–290 (2015)
57. Sareh, P.: The least symmetric crystallographic derivative of the developable double corrugation surface: computational design using underlying conic and cubic curves. *Des. Mater.* (2019). <https://doi.org/10.1016/j.matdes.2019.108128>Get
58. Sareh, P., Guest, S.D.: A framework for the symmetric generalisation of the Miura-ori. *Int. J. Space Struct.* **30**, 141–152 (2015)
59. Chen, Y., Feng, J., Sun, Q.: Lower-order symmetric mechanism modes and bifurcation behavior of deployable bar structures with cyclic symmetry. *Int. J. Solids Struct.* **139–140**, 1–14 (2018)
60. Eriksson, A., Tibert, A.G.: Redundant and force-differentiated systems in engineering and nature. *Comput. Methods Appl. Mech. Eng.* **195**, 5437–5453 (2006)
61. Chen, Y., Yan, J., Feng, J., Sareh, P.: A hybrid symmetry-PSO approach to finding the self-equilibrium configurations of prestressable pin-jointed assemblies. *Acta Mech.* **231**, 1485–1501 (2020)